



## Research Article

# Dielectric Properties, AC Conductivity, and Electric Modulus Analysis of Bulk Ethylcarbazole-Terphenyl

Hussam Bouaamlat <sup>1</sup>, Nasr Hadi,<sup>2</sup> Najat Belghiti,<sup>3</sup> Hayat Sadki,<sup>3</sup>  
Mohammed Naciri Bennani,<sup>3</sup> Farid Abdi,<sup>2</sup> Taj-dine Lamcharfi,<sup>2</sup>  
Mohammed Bouachrine <sup>4</sup>, and Mustapha Abarkan<sup>1</sup>

<sup>1</sup>LSI, Laboratory of Engineering Sciences, Polydisciplinary Faculty of Taza, Sidi Mohamed Ben Abdellah University of Fez, B.P. 1223, Taza, Morocco

<sup>2</sup>LSSC Department of Electrical Engineering, FST, Road Immouzer, Fez-2202, Morocco

<sup>3</sup>Laboratory of Chemistry-Biology Applied to the Environment, Research Team “Applied Materials and Catalyses” Chemistry Department, Faculty of Sciences, Moulay-Ismaïl University, BP 11201 Zitoune, Meknes, Morocco

<sup>4</sup>Natural Substances and Molecular Chemistry Laboratory, Moulay-Ismaïl University, Meknes, Morocco

Correspondence should be addressed to Hussam Bouaamlat; [hussam.bouaamlat@usmba.ac.ma](mailto:hussam.bouaamlat@usmba.ac.ma)

Received 22 October 2019; Accepted 23 December 2019; Published 30 January 2020

Academic Editor: Marinos Pitsikalis

Copyright © 2020 Hussam Bouaamlat et al. This is an open access article distributed under the Creative Commons Attribution License, which permits unrestricted use, distribution, and reproduction in any medium, provided the original work is properly cited.

Electrical and dielectric properties for bulk ethylcarbazole-terphenyl (PEcbz-Ter) have been studied over frequency range 1 kHz–2 MHz and temperature range (R.T –120°C). The copolymer PEcbz-Ter was characterised by using X-ray diffraction. The frequency dependence of the dielectric constant ( $\epsilon'_r$ ) and dielectric loss ( $\epsilon''_r$ ) has been investigated using the complex permittivity.  $\epsilon'_r$  of the copolymer decreases with increasing frequency and increases with temperature. AC conductivity ( $\sigma_{ac}$ ) data were analysed by the universal power law. The behaviour of  $\sigma_{ac}$  increases with increasing temperature and frequency. The change of the frequency exponent ( $s$ ) with temperature was analysed in terms of different conduction mechanisms, and it was found that the correlated barrier-hopping model is the predominant conduction mechanism. The electric modulus was used to analyze the relaxation phenomenon in the material.

## 1. Introduction

Organic conductive and semiconductor materials are emerging as the key materials for future electronics. Organic electronics offer two major advantages over classical inorganic semiconductors. On the one hand, they allow the design of devices on flexible substrates thus offering a wide range of new applications requiring the flexibility of the supports [1]. On the other hand, the costs are lower than those of the inorganic semiconductors. These materials, polymers, for example, can be used in broad assortment applications such as photovoltaic devices [2, 3], field effect transistors [4–6], light-emitting diodes [7–9], and capacitive energy storage [10–12].

The conductivity properties of these assemblies depend on two primary parameters, namely, the efficiency of the transport of charges in the polymer and the efficiency of the interchain transport. The latter often represents the performance-limiting parameter and, consequently, the use of polymers designed for various applications. Recently, different examples of polymers based on  $\pi$ -conjugated backbones have been developed [13–15]. The  $\pi$ -conjugates represent the delocalization or, in other words, the mobility of electrons along the polymer backbone. In conjugated systems, which have alternating double bonds, electron density is delocalized and usually leads to stabilization of the molecule. The mobility of  $\pi$ -electrons contributes to important physical properties as well as to chemical properties of aromatic compounds [16].

Poly(Ethylcarbazole) is a conducting polymer with  $\pi$ -conjugated structure, which has been widely studied and used in photovoltaic and electroluminescent devices due to its excellent thermal stability and electronic properties [17–19]. This polymer exhibits a low dielectric constant over a wide range of temperature and frequency. These low properties can be improved to expand its application fields. To convert poly(ethylcarbazole) into a high  $K$  material, P-terphenyl was used as a building block due to its chemical stability and high dielectric constant [20, 21]. Both materials can be made as an appropriate choice for the study of electrical properties. Theoretical and experimental approaches based on dielectric studies can provide important information which can be used to understand dielectric polarization, dielectric losses, and the behaviour of charge carriers in polymers [22]. The dielectric properties are a source of valuable information on the electrical properties of ions, atoms, and molecules, and most importantly their behaviour within materials. Selvakumar et al. [23] reported that the electronic relaxation process is the only process that occurs in P-terphenyl. Moreover, through the dielectric analysis, they were able to show that the material is continuous and unbroken, meaning that there are no grain boundaries within the polymer, with only a slight amount of impurity and defect concentrations. In addition, the dielectric constant values of P-terphenyl are very high compared to other organic polymers [24]. These high values affect the response time of devices such as solar cells.

In this paper, dielectric properties (dielectric constant and dielectric loss) and electrical properties (ac conductivity and electrical modulus) of poly(ethylcarbazole) and P-terphenyl as a copolymer have been studied as function of temperature and frequency. A strong dependence and correlation between the nature of the material structure and the dielectric properties are found, and therefore, we investigate our copolymer structure using X-ray diffraction technique as an initial step, allowing us to obtain insight into the morphology of the material. Then, we evaluated the real and imaginary parts of dielectric constant, as well as the electrical properties in the temperature range from R.T = 30°C to 120°C and frequency range from 1 kHz to 2 MHz. The different results obtained are discussed according to several theoretical models to determine the most suitable model for interpreting the experimental measurements for PEcbz-Ter.

## 2. Experimental Details

Poly(9-ethylcarbazole) (PEcbz) powder (97%), p-terphenyl (Ter) (99%), ferric chloride ( $\text{FeCl}_3$ ), chloroform  $\text{CHCl}_3$  (99%), and methanol  $\text{CH}_3\text{OH}$  (99.9%) used for the synthesis of the studied compound were purchased from Aldrich chemistry, A Fisher Scientific International and Riedel-de Haën. In this work, the copolymer PEcbz-Ter is dissolved in chloroform (HPLC grade) and oxidatively polymerized with  $\text{FeCl}_3$ .

Dielectric characterization was carried out on a grounded powder of ethylcarbazole-based materials which were pressed by a hydraulic press under  $\sim 50$  MPa to form a pellet with a disk shape. The surface of the pellet is well

polished to dryness and metallized by a thin layer of silver paste in order to obtain two parallel plates; the pellet had the same radius as the electrodes, which are 12 mm in a circular disk shape, and the thickness is 1.75 mm. The real ( $\epsilon_r'$ ) and imaginary ( $\epsilon_r''$ ) parts of the permittivity of this compound are measured in the frequency 1 kHz–2 MHz and temperature range from R.T to 120°C by using the complex impedance spectroscopic technique.

## 3. Theoretical Background

The real ( $\epsilon_r'$ ) and imaginary ( $\epsilon_r''$ ) parts of the permittivity of the material were calculated by using the following formulas:

$$\epsilon_r' = \frac{C_p d}{S \epsilon_0}, \quad (1)$$

$$\epsilon_r'' = \epsilon_r' * \tan(\delta),$$

where  $C_p$  is the capacitance of the sample,  $d$  is the thickness of the disk,  $S$  is the surface area of the electrodes, and  $\epsilon_0 = 8.85 \times 10^{-12}$  F/m is the permittivity of free space. The capacitance ( $C_p$ ) and loss factor ( $\tan(\delta)$  or  $D$ ) can be obtained directly from the measurements. The amplitude of the AC electric signal applied to the samples was 1 V.

The conductivity data were obtained using the following relation [25]:

$$\sigma_{ac} = \epsilon_0 \epsilon_r'' \omega. \quad (2)$$

The AC conductivity is also related to the frequency as [26]:

$$\sigma_{ac} = A \omega^s, \quad (3)$$

where  $A$  is a constant,  $\omega$  is the angular frequency, and  $s$  is the exponent which generally is less than or equal to one. The value and behaviour of the exponent “ $s$ ” versus temperature and/or frequency determine the prevailing conduction mechanism dominant in the material. According to the value of  $s$  and behaviour, several theoretical models have been found to explain the conduction mechanism of materials (QMT, SPT, LPT, and CBH). In the quantum tunnelling model (QMT) [27], “ $s$ ” is anticipated as being frequency-dependent but temperature-independent. In the case of small polaron tunnelling model (SPT) [28], “ $s$ ” is predicted to increase as temperature increases. In large polaron tunnelling (LPT) [29], “ $s$ ” should be both temperature- and frequency-dependent, and in the correlated barrier-hopping CBH model [30] anticipated as being both temperature- and frequency-dependent and “ $s$ ” should decrease with increasing temperature.

In CBH, “ $s$ ” is calculated by using the following formula [31]:

$$s = 1 - \frac{6K_b T}{W_m + K_b T \ln(\omega \tau_0)}, \quad (4)$$

where  $K_b$  is the Boltzmann constant,  $W_m$  is the maximum barrier height, and  $\tau_0$  is the characteristic relaxation time and is in the order of the atomic vibration at period  $10^{-13}$  s [32].

This equation can be approximated to obtain

$$s = 1 - \frac{6K_b T}{W_m} \quad (5)$$

According to this CBH model, the conductivity can be expressed by [33]

$$\sigma_{ac} = \frac{\pi^3}{24} N \varepsilon_r' \varepsilon_0 \omega R_w^6 \quad (6)$$

where  $N$  is the density of localized states at which carriers exist,  $\varepsilon_r'$  is the dielectric constant of the material, and  $R_w$  is the hopping distance and given as

$$R_w = \frac{e^2}{\pi \varepsilon_r' \varepsilon_0 (W_m + K_b T \ln(\omega \tau_0))} \quad (7)$$

Dielectric relaxation mechanism can be obtained from the peak of the dielectric loss ( $\varepsilon_r''$ ), impedance complex, and electric modulus. In the case of the absence of a well-defined peak  $\varepsilon_r''(\omega)$ , the dielectric modulus representation was used to understand and analyze the phenomenon of relaxation in the dielectric materials. This parameter can be defined as [34]

$$M^*(\omega) = \frac{1}{\varepsilon_r' + i\varepsilon_r''}$$

$$M^*(\omega) = M_1 + i * M_2,$$

$$M_1 = \frac{\varepsilon_r'}{\varepsilon_r'^2 + \varepsilon_r''^2} \quad (8)$$

$$M_2 = \frac{\varepsilon_r''}{\varepsilon_r'^2 + \varepsilon_r''^2}$$

## 4. Results and Discussion

**4.1. X-Ray Diffraction.** The X-ray Diffraction (XRD) spectra of the monomers and the synthesized PEcbz-Ter copolymer are shown in Figure 1. The diffractogram of the studied copolymer PEcbz-Ter has characteristic peaks of both the monomers ethylcarbazole (Ecbz) and terphenyl (Ter) such as those located at  $2\theta = 19.1^\circ$ ,  $23^\circ$ ,  $25^\circ$  and  $2\theta = 6.48^\circ$ ,  $13.1^\circ$ ,  $20.35^\circ$ ,  $28^\circ$ ,  $37.58^\circ$ , respectively. The majority of these peaks are intensified markedly, reflecting a new morphology of the copolymer. The existence of fine and intense peaks reflects a structural order in the copolymer and therefore the existence of crystalline regions. The disappearance for the copolymer of the peaks of ethylcarbazole (Ecbz), in particular, in the range of  $2\theta$  between  $10^\circ$  and  $25^\circ$  explains the new structure of the copolymer obtained, which does not necessarily correspond to the presence of the two phases (ethylcarbazole and terphenyl).

**4.2. Dielectric Constant.** The results of dielectric constant for the PEcbz-Ter copolymer with  $\omega$  at different temperatures are illustrated in Figure 2. It shows that the dielectric constant decreases with increasing frequency and increases

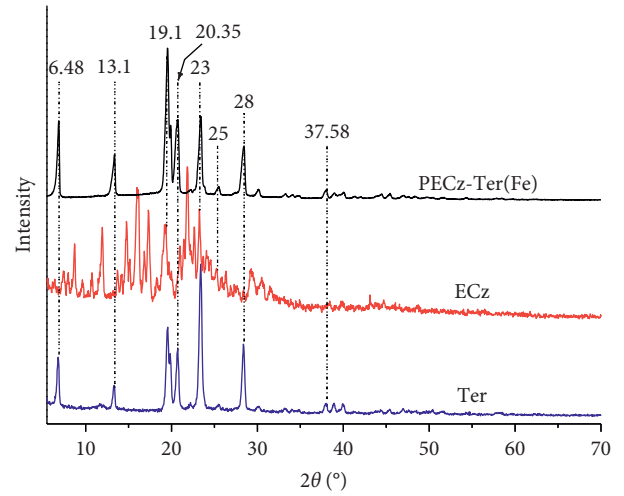


FIGURE 1: X-ray diffraction patterns of terphenyl (Ter), P-ethylcarbazole (PEcbz), and PEcbz-Ter copolymer.

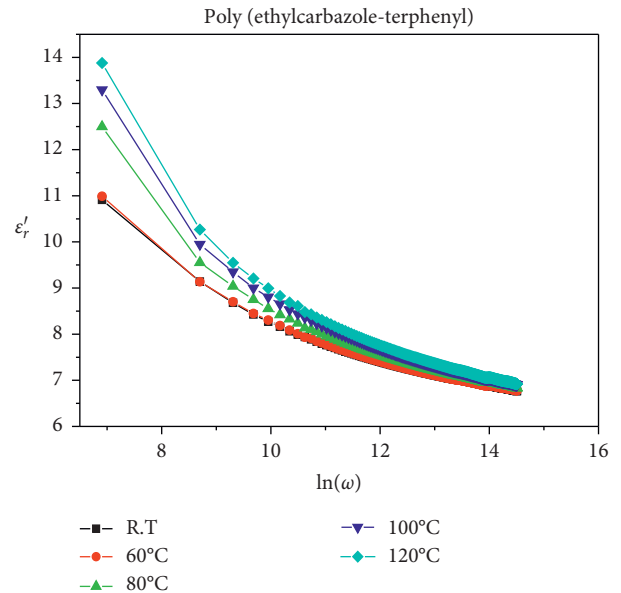


FIGURE 2: Dielectric constant vs. frequency of PEcbz-Ter at different temperatures.

with increasing temperatures at low frequencies. The same behaviour is observed by El-Nahass et al. [35] for p-N,N dimethylaminobenzylidenemalononitrile (DBM) organic dye. It can be noted that, at frequencies above 10 kHz, the permittivity is weakly frequency-/temperature-dependent. At low frequencies, charge carriers respond faster with the externally applied electric field, resulting in the higher value of  $\varepsilon_r'$ . At higher frequencies, charge carriers are unable to follow the rapid changes in the applied electric field, resulting in low values of  $\varepsilon_r'$ . The decrease of dielectric constant with the applied field frequency can be explained based on several types of polarisation (ionic, orientation, and electronic). The ionic polarization due to the application of an electric field on a material induces a displacement of the positive ions relative to the negative ions. This polarization

intervenes for frequencies lower than terahertz. The orientation polarization occurs up to frequencies between 1 kHz and 1 MHz and is related to the structure of the material. Under an applied field, the permanent dipoles of the molecules are oriented in the direction of the field. The electronic polarization is due to the displacement of the electron cloud of the atom with respect to its nucleus. The last one, electron polarization is due to a relative displacement of the nucleus of the atom relative to all the electrons that surround it. This type of polarization is established in a very short time and remains sensitive up to frequencies exceeding those of visible light ( $10^{15}$  Hz). The orientation polarisation is prevalent because it required a longer time compared to other polarizations. Therefore, the value of dielectric constant  $\epsilon_r'$  decreases reaching a constant value at higher frequency corresponding to interfacial polarization. The increase observed in  $\epsilon_r'$  values with temperature is due to the contribution of the charge carriers to the polarization. At low temperatures, polarization is weak due to inability of the dipoles to rotate fast enough; therefore, they oscillate behind the field. The increase in temperature results in sufficient thermal excitation energy obtained by the bound charge carriers, which enhance the polarization leading to the increase in the dielectric constant. Table 1 shows the values of dielectric constant of our copolymer compared with other values in the literature. The dielectric constant is higher than that of many other aromatic organic polymers, making it a good semiconductor material. At the same time, these values are low compared to the results recorded in [26]. This results in a reduced response time.

**4.3. Dielectric Loss.** The imaginary part of the permittivity as a function of frequency at different temperatures calculated by using equation (1) is shown in Figure 3. The behaviour of dielectric loss is similar to the real part of the permittivity, with an anomaly exception at room temperature, which does not have a presently understood origin. The dielectric loss obtained increases with increasing temperature and has a rapid decrease at low frequencies while being almost independent at high frequencies. In Figure 3, the factor loss behaviour as a function of frequency can be explained by the fact that ions migrate within the material at low frequencies. The values of dielectric loss at moderate frequencies are due to the contribution of ion jump and conduction loss of ion migration, as well the ion polarization loss. At high frequency, ion vibrations may be the only source of the dielectric loss, so  $\epsilon_r''$  is frequency-independent.

Differently, the loss factor decreases with increasing frequency and expressed as follows according to the CBH model:

$$\epsilon_r'' = A' \omega^m, \quad (9)$$

where  $A'$  is a constant and  $m$  is the frequency power factor.

From the plot of  $\ln(\epsilon_r'')$  vs.  $\ln(\omega)$ , we can calculate the factor  $m$  and is supposed to be the negative slope of the lines shown in Figure 3(b). According to Guintini model [36], equation (9),  $m$  decreases with increasing temperature, and it is clearly shown in the inset Figure 3(b).

$$m = -\frac{4K_b T}{W_m}. \quad (10)$$

The losses that are attributed to the conduction presumably involve the migration of ions over large distances. This motion is the same as that occurring under DC conditions. The ions jump over the highest barriers in the network. As the ions move, they give some of their energy to the lattice as heat, which accounts for the dissipation of electrical energy as heat.

**4.4. AC Conductivity.** The frequency dependence of the AC conductivity is obtained by equation (2). The plot of conductivity as a function of frequency in the range of 1 kHz to 2 MHz at different temperatures is shown in Figure 4(a). As noted, the behaviour of  $\sigma_{ac}$  that follows our copolymer increases with increasing frequency. The increase in conductivity can confidently be attributed to the hopping mechanism that appears by applying the electrical field. This can be confirmed by studying the behaviour of the frequency exponent in equation (2). Values of “ $s$ ” are calculated from the slope of the linear  $\ln(\sigma_{ac})$  vs.  $\ln(\omega)$ , as depicted in Figure 5. The exponent decreases with increasing temperature; therefore, among all the models discussed in the theoretical background, CBH is the appropriate model for the conduction in our material. Using the values of “ $s$ ” in equation (4), we obtain the yield potential barrier,  $W_m = 0.27$  eV.

Figure 4(b) shows the variation of the AC conductivity as a function of temperature at several frequencies; it is clear that there is a linear relationship between  $\ln(\sigma_{ac})$  and the inverse of temperature. As the temperature rises, AC conductivity increases as well due to the hydrogen bond strength in the molecules, which is affected by the temperature and leads to the movements of thermally excited carriers from energy levels within the band gap.

We report in Table 1 the values of AC conductivity at several temperatures and frequencies for comparison with other values reported in the literature. We defined a new parameter as a figure of merit  $F$  related to the response time, which represents the relationship between the dielectric permittivity and the AC conductivity. The higher its value, the more suitable the material for solar cell applications:

$$F = \frac{\sigma_{ac}}{\epsilon_r}. \quad (11)$$

From Table 1, we can notice that  $F$  for PEcbz-Ter has the highest value at R.T. The straight lines of  $\ln(\sigma_{ac})$  with inverse of temperature follow the Arrhenius equation:

$$\sigma_{ac} = \sigma_0 e^{-E_{ac}/K_b T}, \quad (12)$$

where  $\sigma_0$  is the pre-exponential constant and  $E_{ac}$  is the activation energy. The values of activation energy of our sample calculated as a function of frequency from the slope of the straight lines are plotted in Figure 4(b) and shown in Figure 6. Activation energy  $E_{ac}$  decreases with increasing frequency; this could be due to the applied field frequency that enhances the electronic jumps between the localized

TABLE 1: Dielectric constant  $\epsilon_r'$ , the conductivity  $\sigma_{ac}$ , and the ratio  $F$  at R.T and 120°C for PEcbz-Ter, Ph-PHQ, and P-terphenyl.

Coumpound	Frequency (kHz)	$\epsilon_r'$ at R.T	$\epsilon_r'$ at 120°C	$\sigma_{ac}$ ( $\Omega^{-1}\cdot\text{cm}^{-1}$ ) at R.T	$\sigma_{ac}$ ( $\Omega^{-1}\cdot\text{cm}^{-1}$ ) at 120°C	$F$ ( $\Omega^{-1}\cdot\text{cm}^{-1}$ ) at R.T	$F$ ( $\Omega^{-1}\cdot\text{cm}^{-1}$ ) at 120°C
PEcbz-Ter	11	8.67	9.54	$7.93 \times 10^{-7}$	$1.35 \times 10^{-6}$	$9.15 \times 10^{-8}$	$1.42 \times 10^{-7}$
	600	7.03	7.26	$1.28 \times 10^{-5}$	$1.80 \times 10^{-5}$	$1.82 \times 10^{-6}$	$2.48 \times 10^{-6}$
	2000	6.76	6.91	$3.09 \times 10^{-5}$	$4.39 \times 10^{-5}$	$4.57 \times 10^{-6}$	$6.36 \times 10^{-6}$
Ph-PHQ [25]	0.5	3.92	—	—	—	—	—
	10	2.2	—	$2.2 \times 10^{-10}$	—	$1 \times 10^{-10}$	—
	5000	2	—	$1.4 \times 10^{-8}$	—	$7 \times 10^{-9}$	—
P-Terphenyl [23]	0.15	6670	—	$5.5 \times 10^{-5}$	—	$8.38 \times 10^{-9}$	—
	600	4412	—	—	—	—	—
	1000	4412	—	—	—	—	—

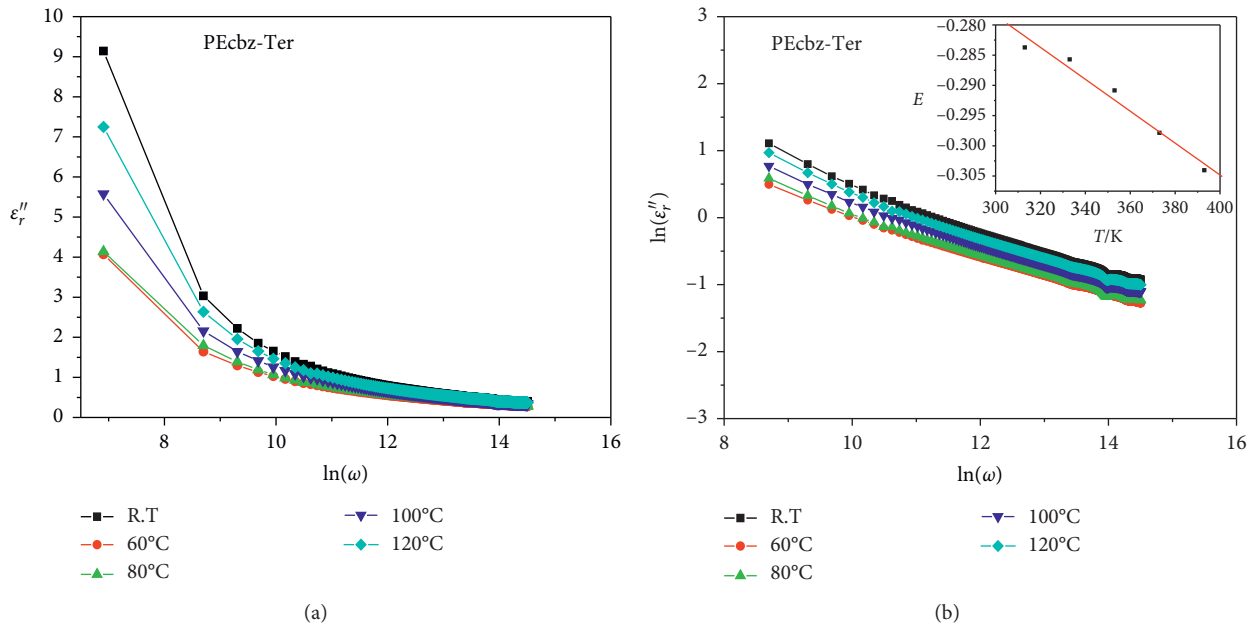


FIGURE 3: (a) Dielectric loss vs. frequency of PEcbz-Ter at different temperatures. (b)  $\ln(\epsilon_r'')$  vs. frequency of PEcbz-Ter at different temperatures.

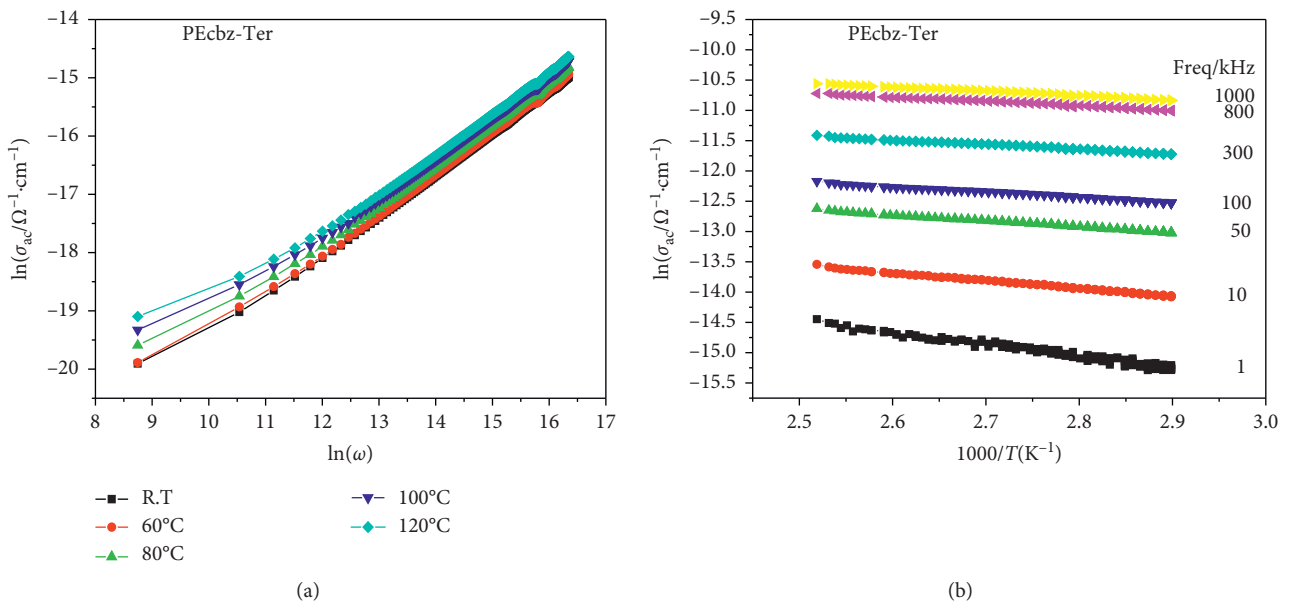


FIGURE 4: (a) AC conductivity vs. frequency of PEcbz-Ter at different temperatures. (b) AC conductivity vs. temperatures of PEcbz-Ter at different frequencies.

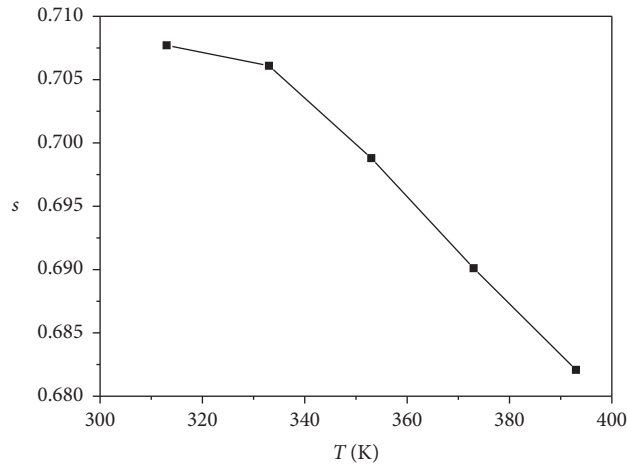


FIGURE 5: Exponent  $s$  as a function of temperature.

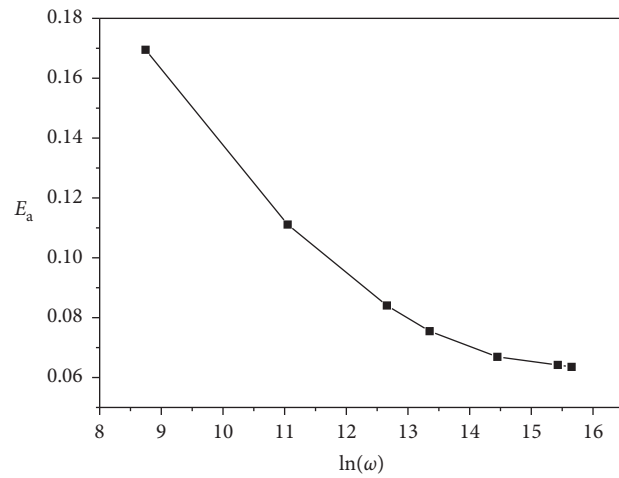


FIGURE 6: Activation energy vs. frequency of PEcbz-Ter.

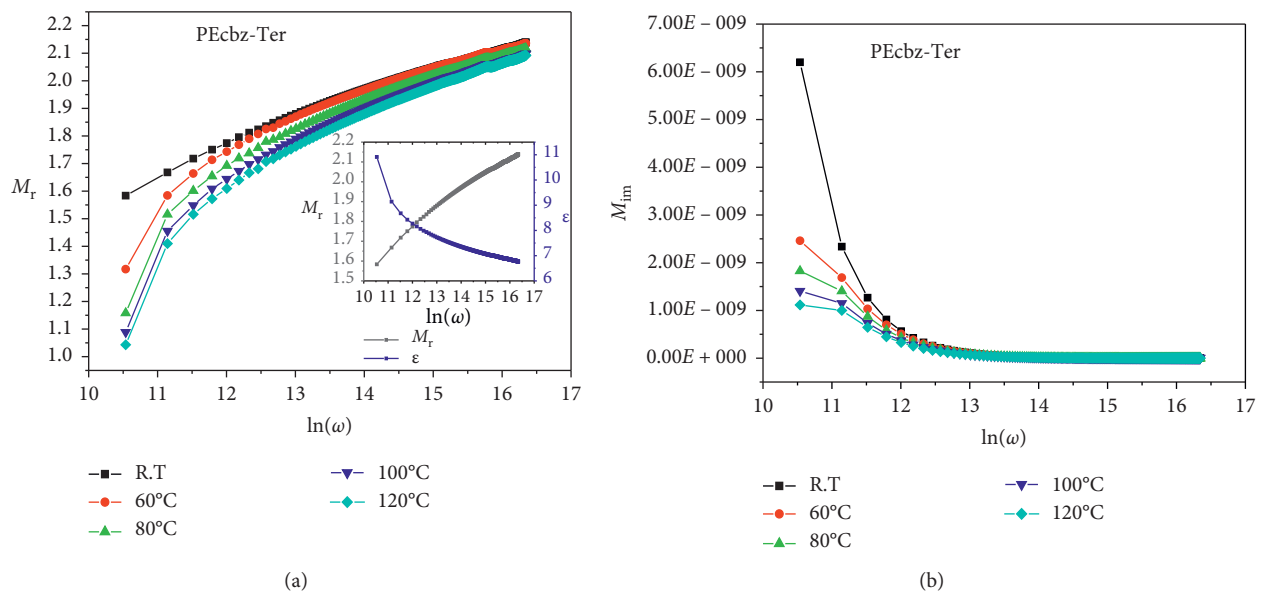


FIGURE 7: (a) Real electrical modulus vs. frequency of PEcbz-Ter at different temperatures. (b) Imaginary electrical modulus vs. frequency of PEcbz-Ter at different temperatures.



states. This confirms that the hopping mechanism controls the transport mechanism.

**4.5. Electric Modulus Analysis.** The complex dielectric modulus  $M^*(\nu)$  is obtained from equation (7) and is depicted in Figure 7(a). From the figure, we observe that  $M_r$  reaches maximum values at high frequencies due to the relaxation process, and it approaches to zero at low frequencies due to the lack of electric polarization. The results showed that dielectric modulus has reverse frequency behaviour compared with dielectric constant at room temperature in inset Figure 7(a), as we can notice from the figure dielectric constant decreases with frequency, while electric modulus is increasing.

The imaginary part of modulus as a function of frequency at few selected temperatures is shown in Figure 7(b). The analysis presented here of  $M_{im}$  suggests the appearance of a dielectric relaxation peak at low frequencies and remains constant with increasing temperature. This behaviour is similar and observed in previous works [37, 38]. The values below the maximum peak are determined by the charge carriers that move on long-range distances, whereas the carriers are confined to potential wells being mobile on short distances determine the values above maximum peak.

## 5. Conclusion

Dielectric constant, dielectric loss, AC conductivity, and electrical modulus of PEcbz-Ter were investigated in the frequency range of 1 kHz–2 MHz and temperature range from R.T to 120°C. X-ray has been done and shows crystalline regions in our polymer. The real part of dielectric constant has strong frequency/temperature dependence at high frequencies, a decrease with increasing frequency, while an increase with increasing temperature at low frequency. The imaginary part of dielectric constant shows similar behaviour to  $\epsilon_r'$  as a function of temperature and frequency. Dielectric loss increases with increasing temperature, and values are below 1% which makes the copolymer suitable for many energy storage applications. The AC conductivity appears to increase with increasing frequency and a decrease with arising temperature. The appropriate model for  $\sigma_{ac}$  was the correlated barrier-hopping (CBH) model. Activation energy decreases with increasing frequency. Those results are promising compared with others in the literature; this could be exploited to investigate more in dielectric and electric properties of organic materials.

## Data Availability

The experimental data used to support the findings of this study will be made available upon request.

## Conflicts of Interest

The authors declare no conflicts of interest.

## Acknowledgments

The authors thank Prof. Alex Brown, Department of Chemistry, University of Alberta, for comments that greatly improved the manuscript.

## References

- [1] B. Mukherjee, "Flexible organic N-channel phototransistor and integrated logic devices," *Optik*, vol. 139, pp. 48–55, 2017.
- [2] H. Luo, J. Lai, C. Wang, and Q. Chen, "Understanding the effects of the energy band alignment at the donor/acceptor interface on the open circuit voltage of organic photovoltaic devices," *Chemical Physics Letters*, vol. 711, pp. 113–117, 2018.
- [3] H. Bronstein, Z. Chen, R. S. Ashraf et al., "Thieno[3,2-b]thiophene-diketopyrrolopyrrole-containing polymers for high-performance organic field-effect transistors and organic photovoltaic devices," *Journal of the American Chemical Society*, vol. 133, no. 10, pp. 3272–3275, 2011.
- [4] T. Takaya, M. D. Mamo, M. Karakawa, and Y.-Y. Noh, "Donor unit effect on DPP based organic field-effect transistor performance," *Dyes and Pigments*, vol. 158, pp. 306–311, 2018.
- [5] D. K. Sagdullina, I. E. Kuznetsov, A. V. Akkuratov, L. I. Kuznetsova, S. I. Troyanov, and P. A. Troshin, "New alternating thiophene-benzothiadiazole electron donor material for small-molecule organic solar cells and field-effect transistors," *Synthetic Metals*, vol. 250, pp. 7–11, 2019.
- [6] G.-W. Hsieh, Z.-R. Lin, C.-Y. Hung, S.-Y. Lin, and C.-R. Yang, "Graphene-induced enhancement of charge carrier mobility and air stability in organic polythiophene field effect transistors," *Organic Electronics*, vol. 54, pp. 27–33, 2018.
- [7] I. Slowik, A. Fischer, H. Fröb, S. Lenk, S. Reineke, and K. Leo, "Novel organic light-emitting diode design for future lasing applications," *Organic Electronics*, vol. 48, pp. 132–137, 2017.
- [8] C. Zhang, X. Qiao, Z. Yang, H. Zhang, and D. Ma, "Highly efficient inverted organic light-emitting diodes with organic p-n junction as electron injection layer," *Organic Electronics*, vol. 58, pp. 185–190, 2018.
- [9] J. C. Germino, J. N. de Freitas, R. A. Domingues, F. J. Quites, M. M. Faleiros, and T. D. Z. Atvars, "Organic light-emitting diodes based on PVK and Zn(II) salicylidene composites," *Synthetic Metals*, vol. 241, pp. 7–16, 2018.
- [10] A. M. Obeidat, M. A. Gharaibeh, and M. Obaidat, "Solid-state supercapacitors with ionic liquid gel polymer electrolyte and polypyrrole electrodes for electrical energy storage," *Journal of Energy Storage*, vol. 13, pp. 123–128, 2017.
- [11] D. G. Atinafu, W. Dong, X. Huang, H. Gao, and G. Wang, "Introduction of organic-organic eutectic PCM in mesoporous N-doped carbons for enhanced thermal conductivity and energy storage capacity," *Applied Energy*, vol. 211, pp. 1203–1215, 2018.
- [12] T. B. Schon, B. T. McAllister, P.-F. Li, and D. S. Seferos, "The rise of organic electrode materials for energy storage," *Chemical Society Reviews*, vol. 45, no. 22, pp. 6345–6404, 2016.
- [13] N. Bouzayen, H. Sadki, M. Mbarek et al., "Synthesis, characterization, DFT and TD-DFT studies of novel carbazole-based copolymer used in high efficient dye-sensitized solar cells," *Polymer Testing*, vol. 66, pp. 78–86, 2018.
- [14] Y. Cai, X. Xue, G. Han et al., "Novel  $\pi$ -conjugated polymer based on an extended thienoquinoid," *Chemistry of Materials*, vol. 30, no. 2, pp. 319–323, 2018.
- [15] D. Keles, M. C. Erer, E. Bolayir et al., "Conjugated polymers with benzothiadiazole and benzotriazole moieties for polymer solar cells," *Renewable Energy*, vol. 139, pp. 1184–1193, 2019.

- [16] Z. M. E. Fahim, S. M. Bouzzine, Y. Ait Aicha, M. Bouachrine, and M. Hamidi, "The bridged effect on the geometric, optoelectronic and charge transfer properties of the triphenylamine-bithiophene-based dyes: a DFT study," *Research on Chemical Intermediates*, vol. 44, no. 3, pp. 2009–2023, 2018.
- [17] S.-Z. Tan, Y.-J. Hu, F.-C. Gong, Z. Cao, J.-Y. Xia, and L. Zhang, "A novel fluorescence sensor based on covalent immobilization of 3-amino-9-ethylcarbazole by using silver nanoparticles as bridges and carriers," *Analytica Chimica Acta*, vol. 636, no. 2, pp. 205–209, 2009.
- [18] S. Bal and J. D. Connolly, "Synthesis, characterization, thermal and catalytic properties of a novel carbazole derived Azo ligand and its metal complexes," *Arabian Journal of Chemistry*, vol. 10, no. 6, pp. 761–768, 2017.
- [19] S. O. Jeon, K. S. Yook, H. S. Son, and J. Y. Lee, "An ethylcarbazole based phosphine oxide derivative as a host for deep blue phosphorescent organic light-emitting diode," *Journal of Luminescence*, vol. 130, no. 11, pp. 2238–2241, 2010.
- [20] E. W. Thulstrup, J. Spanget-Larsen, and R. Gleiter, "The electronic structure of p-terphenyl, 3,6-diphenyl-pyridazine and 3,6-diphenyl-s-tetrazine," *Molecular Physics*, vol. 37, no. 5, pp. 1381–1395, 1979.
- [21] E. Morikawa, Y. Isono, and M. Kotani, "Generation and recombination of charge carriers in p-terphenyl crystal. Photoionization of singlet exciton," *The Journal of Chemical Physics*, vol. 78, no. 5, pp. 2691–2695, 1983.
- [22] G. B. Parravicini, E. R. Mognaschi, D. Comoretto, G. Dellepiane, and A. Brillante, "Dielectric studies on conjugated polymers," *Synthetic Metals*, vol. 101, no. 1–3, pp. 467–468, 1999.
- [23] S. Selvakumar, R. Murugaraj, E. Viswanathan, S. Sankar, and K. Sivaji, "Dielectric properties and relaxation mechanism of organic trans-stilbene and p-terphenyl molecular crystals using impedance spectroscopy," *Journal of Molecular Structure*, vol. 1056–1057, pp. 152–156, 2014.
- [24] A. A. Attia, H. S. Soliman, M. M. Saadeldin, and K. Sawaby, "AC electrical conductivity and dielectric studies of bulk p-quaterphenyl," *Synthetic Metals*, vol. 205, pp. 139–144, 2015.
- [25] H. M. Zeyada, F. M. El-Taweel, M. M. El-Nahass, and M. M. El-Shabaan, "Effect of substitution group on dielectric properties of 4H-pyrano [3, 2-c] quinoline derivatives thin films," *Chinese Physics B*, vol. 25, no. 7, Article ID 077701, 2016.
- [26] M. Pollak and T. H. Geballe, "Low-frequency conductivity due to hopping processes in silicon," *Physical Review*, vol. 122, no. 6, pp. 1742–1753, 1961.
- [27] A. Ghosh, "Transport properties of vanadium germanate glassy semiconductors," *Physical Review B*, vol. 42, no. 9, pp. 5665–5676, 1990.
- [28] D. L. Tonks and R. N. Silver, "Small-polaron models for the hydrogen-concentration dependence of hydrogen diffusion in Nb," *Physical Review B*, vol. 26, no. 12, pp. 6455–6469, 1982.
- [29] A. Ghosh, "Ac conduction in iron bismuthate glassy semiconductors," *Physical Review B*, vol. 42, no. 2, pp. 1388–1393, 1990.
- [30] G. E. Pike, "Ac conductivity of scandium oxide and a new hopping model for conductivity," *Physical Review B*, vol. 6, no. 4, pp. 1572–1580, 1972.
- [31] A. R. Long, "Frequency-dependent loss in amorphous semiconductors," *Advances in Physics*, vol. 31, no. 5, pp. 553–637, 1982.
- [32] R. F. Loane, P. Xu, and J. Silcox, "Thermal vibrations in convergent-beam electron diffraction," *Acta Crystallographica Section A Foundations of Crystallography*, vol. 47, no. 3, pp. 267–278, 1991.
- [33] S. R. Elliott, "A.c. conduction in amorphous chalcogenide and pnictide semiconductors," *Advances in Physics*, vol. 36, no. 2, pp. 135–217, 1987.
- [34] A. Oueslati, F. Hlel, K. Guidara, and M. Gargouri, "AC conductivity analysis and dielectric relaxation behavior of  $[N(C_3H_7)_4]_2Cu_2C_{16}$ ," *Journal of Alloys and Compounds*, vol. 492, no. 1–2, pp. 508–514, 2010.
- [35] M. M. El-Nahass, A. A. Atta, M. A. Kamel, and S. Y. Huthaily, "AC conductivity and dielectric characterization of synthesized p-N,N dimethylaminobenzylidenemalononitrile (DBM) organic dye," *Vacuum*, vol. 91, pp. 14–19, 2013.
- [36] J. C. Giuntini, J. V. Zanchetta, D. Jullien, R. Eholie, and P. Houenou, "Temperature dependence of dielectric losses in chalcogenide glasses," *Journal of Non-crystalline Solids*, vol. 45, no. 1, pp. 57–62, 1981.
- [37] F. Yakuphanoglu, "Electrical conductivity and electrical modulus properties of  $\alpha$ ,  $\omega$ -dihexylsexithiophene organic semiconductor," *Physica B: Condensed Matter*, vol. 393, no. 1–2, pp. 139–142, 2007.
- [38] S. I. Qashou, A. A. A. Darwish, M. Rashad, and Z. Khattari, "AC electrical conductivity and dielectric relaxation studies on n-type organic thin films of N, N'-Dimethyl-3,4,9,10-perylene-dicarboximide (DMPDC)," *Physica B: Condensed Matter*, vol. 525, pp. 159–163, 2017.